J. Fluid Mech. (2008), *vol.* 600, *pp.* 257–269.
doi:10.1017/S0022112008000475 Printed in the United Kingdom

Molecular mechanisms of liquid slip

A. MARTINI[1], A. ROXIN[2], R. Q. SNURR[3], Q. WANG[4] AND S. LICHTER[4]

[1]School of Mechanical Engineering, Purdue University, West Lafayette, IN 47907, USA

[2]Departament de Tecnologia, Universitat Pompeu Fabra, Barcelona, Spain

[3]Department of Chemical and Biological Engineering, Northwestern University, Evanston, IL 60208, USA

[4]Department of Mechanical Engineering, Northwestern University, Evanston, IL 60208, USA

(Received 10 September 2007 and in revised form 26 December 2007)

It is now well-established that the liquid adjacent to a solid need not be stationary – it can slip. How this slip occurs is unclear. We present molecular-dynamics (MD) simulation data and results from an analytical model which support two mechanisms of slip. At low levels of forcing, the potential field generated by the solid creates a ground state which the liquid atoms preferentially occupy. Liquid atoms hop through this energy landscape from one equilibrium site to another according to Arrhenius dynamics. Visual evidence of the trajectories of individual atoms on the solid surface supports the view of localized hopping, independent of the dynamics outside a local neighbourhood. We call this defect slip. At higher levels of forcing, the entire layer slips together, obviating the need for localized defects and resulting in the instantaneous motion of all atoms adjacent to the solid. The appearance of global slip leads to an increase in the number of slipping atoms and consequently an increase in the slip length. Both types of slip observed in the MD simulations are described by a dynamical model in which each liquid atom experiences a force from its neighbouring liquid atoms and the solid atoms of the boundary, is sheared by the overlying liquid, and damped by the solid. In agreement with the MD observations, this model predicts that above a critical value of forcing, localized slipping occurs in which atoms are driven from low-energy sites, but only if there is a downstream site which has been vacated. Also as observed, above a second critical value, all the liquid atoms adjacent to the wall slip. Finally, the dynamical equation predicts that at extremely large values of forcing, the slip length approaches a constant value, in agreement with the MD simulation results.

1. Introduction

The no-slip condition remains a trustworthy boundary condition for large-scale Newtonian flows. However, it is now well-established that the liquid adjacent to a solid can slip, i.e. have a non-zero velocity relative to the bounding solid (see the reviews by Neto *et al.* 2005; Lauga, Brenner & Stone 2005; Bocquet & Barrat 2007). Furthermore, for small-scale geometries this slip can be significant. Holt *et al.* (2006) and Majumder *et al.* (2005) find that flow through their nanometre-diameter channels is nearly frictionless. Flows through micro- and nano-scale channels offer possibilities for sorting solute molecules by size and other properties. For example, semi-permeable membranes have been used for years as a means of desalination. The utility of small

pores to sort molecules by size and chemical properties is limited, however, by their extremely high flow resistance. The presence of slip and concomitant reduced drag offer the prospect of dramatically reduced energy costs that may make a wide range of separation processes economically feasible (see Urbakh *et al.* 2004; Eijkel & van den Berg 2005; Sholl & Johnson 2006).

Slip is often viewed from the perspective of its gross properties, such as slip length, which is (as described below) an average over all the liquid molecules near the solid boundary. For revealing the dynamics of slip, these averaged measures are ambiguous. For example, the same slip length can arise due to the fast motion of a single liquid molecule as well as from the slow downstream drift of many molecules. So, although slip has been well-documented, the means by which slip occurs is virtually unknown. The work described here presents evidence for particular molecular mechanisms. We find that at low forcing, at any instant, slip is due to the motion of only a few molecules which propagate along the liquid–solid interface as a localized nonlinear mode: we call this 'defect slip'. At high forcing, the means of motion is different: at any time, all molecules adjacent to the boundary contribute equally to slip: we call this 'global slip'.

In §§ 3.1–3.4, we present four types of molecular-scale evidence that at low forcing slip is a due to localized defect motion: the existence of a ground state, the existence of a transition state between ground states, visual molecular evidence of slip motion, and measurements of the small fraction of interfacial atoms which contribute to slip. We also find a second mechanism of slip, which makes its appearance at higher forcing. Evidence for this global slip is presented in §§ 3.3–3.5. In § 4 we review a molecular-level dynamical model of slip and compare its predictions with our simulation's findings. The analytical model and simulation concur in showing (i) a critical value of forcing required for the commencement of defect slip, (ii) a second critical value marking global slip, and (iii) a high-forcing region over which the slip length is constant. The paper concludes in § 5 with an overview of the findings. We begin with a discussion of our molecular dynamics simulation methodology.

2. Simulation methodology

We used non-equilibrium molecular-dynamics (MD) simulations in a planar Couette geometry. The walls consisted of atoms forming four planes of a face-centred-cubic lattice, where each atom was tethered to its lattice site by a linear spring. The distance between the mean centre of mass of the innermost wall atoms, or channel height, was 3 nm (with the exception of the data in the inset to figure 2). Periodic boundary conditions were applied in the flow direction and transverse to the wall-normal direction.

The simulated liquid was n-decane using a united atom model (i.e. each molecule is composed of ten monomers connected by rigid bonds) and allowing for both bond bending and torsion. To avoid confusion with the n-decane *molecule*, each united atom, or monomer, is referred to in the text simply as an *atom*.

In general, the liquid was sheared by moving the top and bottom bounding walls at equal and opposite speeds $\pm U$ between 1 and 1000 m s^{-1}. The one exception to this was for the data collection used for figure 3, in which one wall was held stationary to facilitate tracking of atoms. For consistency, all wall speeds are reported in a frame of reference in which the walls move with equal and opposite speed U.

All non-bonded interactions were modelled using Lennard–Jones potentials parameterized by energy ϵ and length σ scales. For interactions between two atoms of the same type, the length parameters were $\sigma_{CH_3} = 0.377$ nm, $\sigma_{CH_2} = 0.393$ nm, and

$\sigma_{wall} = 0.266$ nm, and the energy parameters were $\epsilon_{CH_3}/k_B = 98.1$ K, $\epsilon_{CH_2}/k_B = 47.0$ K, and $\epsilon_{wall}/k_B = 529.3$ K, where k_B is Boltzmann's constant. Parameters for interactions between different atom types were calculated using the Lorentz–Berthelot mixing rules (hereafter subscripts *LL* and *LS* will indicate liquid–liquid and liquid–solid interaction parameters, respectively). The liquid was allowed to heat up due to shear, while the temperature of the walls was maintained at 300 K using a Nosé-Hoover thermostat. Following equilibration, simulations were run with a time step of 10^{-6} ns to a minimum duration of 1 ns.

A key factor that differentiates this study from others previously reported is that the fluid density was determined using a grand canonical (i.e. constant temperature, volume, chemical potential) Monte Carlo simulation. As the chemical potential, rather than particle number, is fixed, the liquid is allowed to reach equilibrium in a way that models the density that would be present if the channel were filled from a reservoir at the given temperature. At a channel width of 3 nm, the simulation contained 96 n-decane molecules. Additional simulation details are given in Martini *et al.* (2006).

It is frequently observed that the continuum equations of fluid dynamics hold within the interior of the liquid and that the slip speed is due entirely to a discontinuity in speed between the wall and the adjacent liquid (see Thompson & Troian 1997). So, the liquid atoms adjacent to the wall have a special status: we call these atoms the first liquid layer. More precisely, we define the first liquid layer as being composed of all liquid atoms whose centres of mass lie between the wall and the first minimum in the average liquid density profile. Density and velocity profiles are calculated by averaging the number and velocity of atoms in discrete 'bins' parallel to the channel walls. The amount of slip is typically quantified in terms of the slip length, $L_s = v_s/\dot{\gamma}$. The mean shear rate, $\dot{\gamma}$, is determined by fitting a straight line to the average velocity profile in the central part of the channel, where the central region includes all bins except those lying within the first liquid layer. The slip speed, v_s, is determined as the difference between the wall speed and $\dot{\gamma}$ extrapolated to the wall.

3. Molecular mechanisms of slip

3.1. *The ground state*

Liquid density varies tangentially along a solid surface with a length scale of approximately the lattice spacing (see Thompson & Robbins 1990; Lichter, Roxin & Mandre 2004). This density variation can be understood by noting that a liquid molecule traversing at constant height over a solid surface would experience a fluctuating potential as it passes over the lattice of discrete solid atoms (see Steele 1973). This inhomogeneous potential offers sites of low energy which the liquid atoms preferentially occupy, leading to the observed variations in liquid density. Whether or not this tangential variation plays an active role in the dynamics of slip can be tested by determining whether it provides a measurable ground state for motion.

The ground state is the configuration of liquid atoms in the first liquid layer that has a lower energy than any other configuration. Say there are N atoms in their ground-state configuration. As this is the preferred configuration, diffusion from the bulk into and out of the first liquid layer will be biased such that departures away from N are discouraged. On the other hand, in the absence of a ground state, the arrival and departure of liquid atoms at the solid surface are unbiased. The dynamics of N can be made equivalent to a random walk by determining the change in N from one time step to the next: changes of $(+1, -1, 0)$ atoms are analogous to (right, left, in-place) random steps, and so summing the changes in N is analogous to the

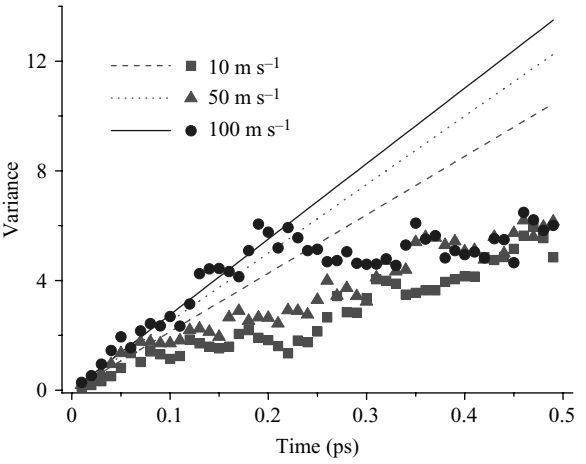

FIGURE 1. Variance in the number of atoms in the first liquid layer as a function of time for wall speeds of 10, 50, and 100 m s^{-1}. The lines show a linear increase of variance with time, as would be seen in the absence of a ground state. The symbols are the variance observed in the MD simulations. After an initial rise following the appropriate line, the variance falls below the line, as would be expected for diffusion in the presence of a ground state. See Appendix A for the calculations used to determine the variance.

distance travelled in a random walk (see Appendix A). The simple random walk is often portrayed as a drunk staggering to the right or left from a lamppost. When a ground state is present, the biased diffusion can be envisioned as a drunk restrained to the lamppost with an elastic tether, which pulls him back (to his ground state) as he tries to wander too far. The liquid–solid interface, then, can be queried for the presence of a dynamically active ground state by measurement of the variance in N: if the dynamics of the adjacent liquid atoms are unaffected by the substrate potential, then the variance in their number will increase linearly in time. If the presence of a ground state affects the dynamics, the variance will be restrained such that, for long enough time, it will be sublinear (Appendix A). Three representative data sets are shown in figure 1. The variance in the number of liquid atoms adjacent to the solid follows the linear prediction for short times, before a sufficient number of steps have been taken to move far from the ground state: in the picturesque language of the staggering drunk, the tether is not yet stretched. Given sufficient time, the variance falls below the linear simple-random-walk prediction, revealing the presence of a ground state.

The ground state is a prerequisite for a particular mode of molecular motion, the propagation of defects, as we now discuss.

3.2. *Liquid slip as a rate process*

Let the low-energy positions occupied by each first-liquid-layer atom when in the ground-state configuration be called equilibrium sites. Consider that the ground-state configuration is altered by the removal – via diffusion into the bulk – of one atom from its equilibrium site. If an atom from an adjacent equilibrium site now hops over to fill this vacancy, a new vacant site is created at the location that it vacated. In this way, liquid atoms can sequentially hop along the liquid–solid interface until the ground state is restored by the diffusion of an atom from the bulk into the vacancy. This is the basic process of defect slip. Precedent for this process can be found in Tolstoi (see Blake 1990) and in a model of the advancing contact line (see Hoffman

1983). (The ground state can also be perturbed by an additional atom which diffuses from the bulk into the ground state. This case can be treated similarly to case of a vacancy. Either the removal or the addition of an atom into the ground state – generating either a vacancy or a crowding – creates what we refer to as a defect.)

On any real interface, or in any reasonably sized MD simulation, there will be more than one vacancy which perturbs the ground state. However, if the vacancies are sufficiently far apart, then each one propagates independently of the others. So, it is sufficient to focus on the hopping of a single atom from one equilibrium site to another, as can be modelled using transition-state theory (see Glasstone, Laider & Eyring 1941; Lichter *et al.* 2007).

A liquid atom in its equilibrium site is assigned a Gibbs free energy, $G = \mathscr{U} + P\mathscr{V} - TS$, where $\mathscr{U}$ is the internal energy, P is pressure, $\mathscr{V}$ is volume, T is temperature and S is entropy. As a liquid atom moves from one equilibrium site to another, it passes through a location of higher energy. The highest (lowest) energy encountered is assigned $G^{\ddagger}$ (G^{o}). The downstream hopping of an atom from one equilibrium site to another is equivalent to the upstream hopping of a vacancy: as an atom hops into an unoccupied downstream site, its upstream initial position becomes vacated.

The rate of hopping from one site to the other is given by $\omega \propto \exp(-\Delta G^{\ddagger}/(k_B T))$, where $\Delta G^{\ddagger} = G^{\ddagger} - G^{o}$ (see Hanggi, Talkner & Borkovec 1990; Glasstone *et al.* 1941). Each hop makes a contribution to the amount of slip. If there are many hops simultaneously occurring over the surface of the solid, then the slip speed v_s is given by the mean number of vacancies times their mean rate of hopping, ω, times the length per hop. For a given wall speed, as the channel height is varied, we assume that the adiabatic component $\mathscr{U}$ and the entropic term TS are constant, leaving only the pressure–volume contribution to the free energy change. We also assume that the number of vacancies is at most weakly dependent on the pressure and shear rate, and so find that $v_s \propto \omega$ (see Lichter *et al.* 2004). Then

$$\frac{v_s(P)}{v_s(P_0)} = \exp\left[-\frac{(P - P_0)\Delta\mathscr{V}^{\ddagger}}{k_B T}\right], \tag{3.1}$$

where $\Delta\mathscr{V}^{\ddagger}$ is the change of volume between the transition state and the equilibrium site, P is the solvation pressure for a given channel height, and P_0 is a conveniently chosen reference solvation pressure (see Lichter *et al.* 2007). Solvation pressure is the excess above the isotropic bulk pressure of the normal pressure at the wall. In nano-confined fluids it is non-zero, arising due to the distribution of the finite-sized liquid molecules being altered by the presence of the solid (see Horn & Israelachvili 1981). The temperature and solvation pressure are measured for each channel height between 1 and 3 nm from our simulation. To estimate the change in volume, we follow Glasstone *et al.* (1941) and consider that the volume of the vacancy in the transition state is smaller than that in the equilibrium site, hence the negative sign in $\Delta\mathscr{V}^{\ddagger} = -f(4\pi/3)(\sigma_{LS}/2)^3$, where $0 \leqslant f$. The value for f is a fitting parameter. A comparison of the prediction from (3.1) to data is shown for a wall speed of $50\,\mathrm{m\,s^{-1}}$ in the inset of figure 2. Equation (3.1) does reasonably well in matching both the amplitude and phase of the oscillatory variations in slip length with channel height. This suggests that transition-state hopping is the dominant process at these low forcings.

The fitting factor, f, in (3.1) is proportional to the size of the transition state. For wall speeds up to about $100\,\mathrm{m\,s^{-1}}$, f remains sizeable, as expected when the dominant means of slip is due to defects. At wall speeds above about $100\,\mathrm{m\,s^{-1}}$, the

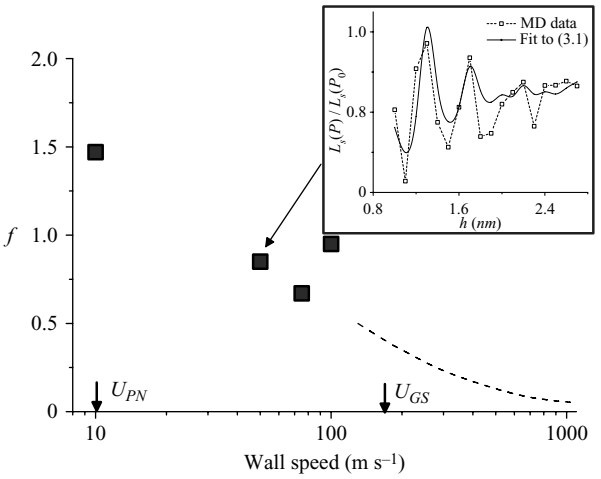

FIGURE 2. The fitting factor f from (3.1) as a function of wall speed. As shown in the inset for a wall speed of 50 m s^{-1}, (3.1) relates variations in slip length to the measured solvation pressure $P(h)$ by assuming that the liquid atoms hop along the liquid–solid interface by a transition-state process. As described in the text, the factor f is proportional to the size of the transition state. Estimates for the Peierls–Nabarro transitions to defect slip U_{PN} and global slip U_{GS}, as determined in the text, are marked on the abscissa. $O(1)$ values of f can be expected throughout the range in which defect slip is the dominant mechanism of slip, as can be seen on the figure. Above U_{GS} global slip becomes the dominant mechanism of slip, and here we find that there is no significant correlation between pressure and slip speed. This can be explained by $f \to 0$ as the wall speed increases, as speculated in the figure by a dashed line.

variations in slip speed with channel height become uncorrelated with the solvation pressure and we can no longer determine f. This can be interpreted as there no longer being a measurable transition state, suggesting that f goes to zero, as shown by the dashed line in figure 2. The process which supersedes hopping at high wall speeds is introduced in § 3.3.

3.3. *Visual analysis*

For wall speeds of 0.5, 5, 50, and 500 m s^{-1}, individual atoms of the n-decane molecule were tracked while they remained in the first liquid layer, see figure 3. These wall speeds present different qualitative types of molecular motion. At the lowest wall speed, there is very little slip (also illustrated in figure 5). As would be exactly true in the no-slip case, an atom is nearly equally likely to move either upstream or downstream. At a wall speed of 5 m s^{-1}, the atoms remain in one equilibrium site, shown by the nearly horizontal portions of its trajectory, but then rapidly move to another site. The trajectories for three atoms, from different n-decane molecules, are shown. Note that each atom's movement is independent of the motion of the other atoms. As the wall speed is increased to 50 m s^{-1}, the atomic motion retains some features similar to that seen at 5 m s^{-1}. In particular, the motion of atoms on different molecules is, at times, independent as the atoms alternate between resting in their equilibrium sites and hopping downstream. However, at other times, the atoms appear to move in a collective manner, all atoms slipping downstream at the same speed. At the highest wall speed, 500 m s^{-1}, the independent hopping of atoms is overwhelmed. As indicated by the parallel trajectories, collective motion in which all atoms persistently move downstream at the same speed becomes the dominant motion. This is called global slip.

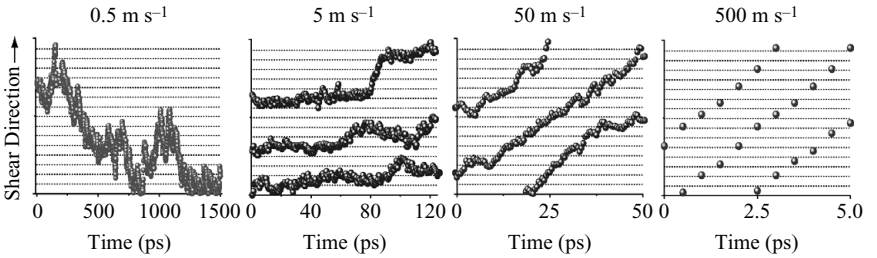

FIGURE 3. Trajectories of atoms in the first liquid layer relative to the wall for wall speeds of $0.5\,\mathrm{m\,s^{-1}}$, $5\,\mathrm{m\,s^{-1}}$, $50\,\mathrm{m\,s^{-1}}$, and $500\,\mathrm{m\,s^{-1}}$. The horizontal dotted lines show the spacing of the solid atoms of the wall. Horizontal portions of the trajectory signify that the atom is stationary relative to the wall. A single trajectory is shown for $0.5\,\mathrm{m\,s^{-1}}$; the three trajectories at the higher wall speeds are from non-neighbouring atoms on different n-decane molecules. Some trajectories have been shifted vertically for clarity. At the lowest wall speed, the atoms are nearly equally likely to move upstream or downstream. At a wall speed of $5\,\mathrm{m\,s^{-1}}$, the atoms alternate between remaining nearly stationary and moving downstream. At $50\,\mathrm{m\,s^{-1}}$, the intervals of downstream motion increase. At $500\,\mathrm{m\,s^{-1}}$, all atoms move with equal speed over the solid, yielding parallel trajectories.

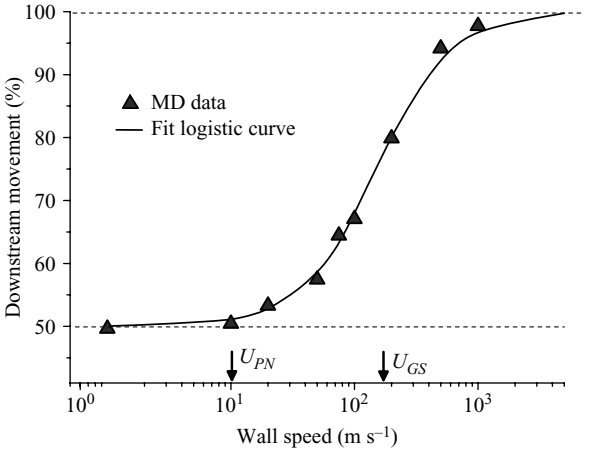

FIGURE 4. Long-time averages of the percentage of atoms in the first liquid layer that are moving downstream at a given wall speed. Symbols correspond to simulation data while the solid line represents a logistic function of the form $0.5 - 0.5/(1 + (U/U_0)^{\alpha})$ where the centre point, $U_0 = 148\,\mathrm{m\,s^{-1}}$ and the exponent, $\alpha = 1.53$ are fitted to the data using nonlinear least squares. The estimates for the transitions to defect slip U_{PN} and global slip U_{GS}, as determined in the text, are marked on the abscissa.

3.4. *Percent participation*

For the no-slip condition, the average atomic motion should be 50 % downstream and 50 % upstream. In the other extreme of global slip, the average atomic motion should approach 100 % downstream movement. Defect slip should take place with some percentage between these limits. These predictions are validated by the simulation data shown in figure 4. We interpret the initial increase in percentage of downstream motion as due to defect slip. Note that, due to our measurement technique, even if an atom is confined to oscillate about an equilibrium position, it would alternately be considered as part of the forward or backward population of atoms as it oscillated.

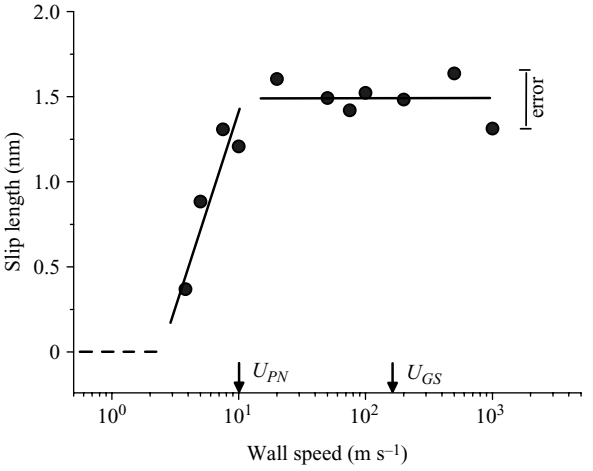

FIGURE 5. Slip length as a function of wall speed. As an aid to the eye, a straight line is fitted to the data for $U \lesssim 20\,\mathrm{m\,s^{-1}}$. To compare with the vdFK prediction that the slip length approaches a constant value at high forcing, a line of zero slope is fit to the data for $U \gtrsim 20\,\mathrm{m\,s^{-1}}$. The estimates for the transitions to defect slip U_{PN} and global slip U_{GS}, as determined in the text, are marked on the abscissa. The maximum error in the slip length calculation for $U > 20\,\mathrm{m\,s^{-1}}$ is indicated by the error bar.

By comparing figures 2 and 4, it can be seen that measurable values of f, indicative of defect slip, occur in the interval of wall speeds within which the percentage of downstream motion begins to rise. Within this range of wall speeds, the percentage of atoms engaged in slip remains small, consistent with the view of defect slip as a localized disturbance in which most atoms remain oscillating about their equilibrium positions and do not slip. On the other hand, at a wall speed of several hundred $\mathrm{m\,s^{-1}}$, the percentage approaches 100 %, consistent with the view of global slip shown in the final frame of figure 3. Now, vacancies are no longer needed for slip and so we expect that f should decrease to zero in this range, as was shown in figure 2.

3.5. *Slip length*

The slip length was calculated as a function of wall speed, as shown in figure 5. The slip length increases with wall speed for speeds up to about $20\,\mathrm{m\,s^{-1}}$, and thereafter appears to remain relatively constant.

4. Frenkel–Kontorova model for liquid slip

Previously, we introduced a theoretical model for slip (see Lichter *et al.* 2004) which describes the dynamics of the atoms in the first liquid layer of a two-dimensional flow,

$$m\ddot{x}_i = -\frac{2\pi g}{\lambda}\sin\left(\frac{2\pi x_i}{\lambda}\right) + k(x_{i+1} - 2x_i + x_{i-1}) + \eta_{LL}(V - \dot{x}_i) - \eta_{LS}\dot{x}_i. \qquad (4.1)$$

Reading the equation from left to right, we find that the mass m times acceleration $\ddot{x}_i$ of the ith atom along the x-direction is due to the force caused by a potential field of strength g which arises from the linear array of solid atoms with spacing λ (see Appendix B), the interactions of strength k from the nearest-neighbour liquid atoms at $i+1$ and $i-1$, the force due to shear from the liquid layer above, which is

moving at speed $V = \dot{\gamma}(h/2 - 2d)$, and finally, the force due to friction, with friction coefficient η_{LS}, due to slip along the wall. The strength of the liquid–liquid interaction k is determined by fitting a quadratic potential to the liquid–liquid Lennard–Jones potential. It is found that $k = 72\epsilon_{LL}/(2^{4/3}\sigma_{LL}^2)$. The coefficient $\eta_{LL} \equiv \mu(\mathscr{A}/d)/N$ is the bulk viscosity μ times a coefficient to apportion the continuum viscosity coefficient to the discrete liquid atoms, where $\mathscr{A}/N$ is the area per liquid atom in the first liquid layer, and d is the liquid–liquid spacing normal to the surface.

Equation (4.1) is a form of the well-known Frenkel–Kontorova equation which models the interaction of two lattices (see Braun & Kivshar 1998). What is novel in this application to liquids, is that the set of atoms i changes in time as atoms diffuse into and out of the first liquid layer. This diffusion is incorporated into the model by stochastically adding or removing atoms (see Lichter *et al.* 2004). The diffusion changes the number of liquid atoms instantaneously in the system, so we call the complete set of equations the variable-density Frenkel–Kontorova (vdFK) model. The vdFK model can be solved numerically or approximated analytically (see Braun & Kivshar 1998; Roxin 2004). At low values of the forcing parameter V, there are no propagating solutions as the liquid atoms become trapped near the minima of the solid potential. For higher values of the forcing, soliton solutions of propagating localized modes appear. At still higher forcing levels, the entire first liquid layer can slip. There are well-defined transitions (see Braun & Kivshar 1998) between the occurrence of non-propagating solutions, solitons, and global slip, which we now compare with our MD observations.

4.1. *The transition to global slip*

The vdFK equation predicts a transition to global slip in which all atoms move with nearly constant speed. Consequently, the acceleration term in (4.1) drops out. In addition, adjacent atoms keep their relative displacement so there is no contribution to the force from intermolecular interactions. Furthermore, just at the transition, the speed is small. Hence, the terms remaining in (4.1) yield the criterion for transition, namely that the forcing term balances the substrate potential,

$$V_{GS} = \frac{2\pi g(l)}{\lambda \eta_{LL}}, \tag{4.2}$$

where l is the height of the first liquid layer (see Appendix B). We find that this value of forcing V_{GS} occurs at a wall speed $U_{GS} \simeq 170\,\mathrm{m\,s^{-1}}$, which is marked on figures 2, 4 and 5. The vacancy volume, as measured by f, is an intrinsic part of defect slip, but does not play a necessary role in global slip. Hence, we would expect that U_{GS} should occur in the region where f falls off rapidly, as is observed in figure 2. Global slip involves all the liquid atoms adjacent to the boundary. Therefore, at the transition, we would expect that there is a rapid rise in the percentage of the atoms moving forward. The value of U_{GS}, as marked on figure 4 bears this out. The value for U_{GS} compares well with the value $U_0 = 148\,\mathrm{m\,s^{-1}}$ found from the logistic fit to the figure 4 data. And, lastly, we see that the parallel trajectories indicative of global slip in figure 3 occurs at $U = 500\,\mathrm{m\,s^{-1}}$, above the predicted transition to global slip.

There are two caveats to keep in mind in interpreting this transition and the one to be discussed below in § 4.2. First, the liquid atoms adjacent to the boundary are not all at precisely the same height, but rather there is a range of heights. We find that the density peak nearest to the wall (located at $l = 0.34\,\mathrm{nm}$ for the case shown in figures 2 and 4) has a width of $\pm 0.035\,\mathrm{nm}$ at half-height. Atoms at different heights l will experience a different amplitude of substrate potential, which we explicitly show

by writing $g(l)$ in (4.2). This distribution of heights will lead to a distribution of values for U_{GS}. So, the single value presented is only indicative of where the transition lies. Secondly, the vdFK equation (4.1) treats the dynamics of the liquid atoms as if flow were one-dimensional. However, the MD simulations are for a full three-dimensional liquid. Once again, this suggests that the values derived from the vdFK model should not be used as a quantitative measure, but only as a guide.

4.2. *The transition from no-slip to defect slip*

The transition to defect slip, within the context of FK equations, is called a Peierls–Nabarro transition (see Braun & Kivshar 1998; Zhu & Granick 2002 also give experimental evidence in support of a transition from no-slip to slip). The forcing required for this transition is less than that for global slip, discussed above, due to the helpful contribution of forces from nearest-neighbour liquid–liquid interactions. The critical forcing needed for defect slip can be simply estimated, in the limiting case of small forcing and where the liquid size is commensurate with the solid lattice spacing, as follows (see Floría & Mazo 1996). Consider liquid atoms each occupying a low-energy equilibrium site at the bottom of the periodic solid potential. This regular placement is then locally perturbed by the departure, into the bulk, of a single liquid atom, creating a vacancy at one equilibrium site. The liquid atom just upstream of the vacancy can hop into it while all other liquid atoms remain nearly stationary. To hop from one equilibrium site to another, an isolated atom, or equivalently an atom with no liquid–liquid interactions (i.e. $k=0$), would need the forcing as calculated in the previous section for the global slip transition. Here, however, the vacancy leads to an imbalance of the liquid–liquid forces. Hence, the dominant balance within (4.1) is among the terms accounting for the solid potential, the forcing, and, additionally, the liquid–liquid interaction. The liquid–liquid term needs to properly account for the perturbation in the configuration of the ground state due to the changes in position of the atoms neighbouring the vacancy. Accounting for these changes, Braun, Kivshar & Zelenshkaya (1990) report that the value at which defect slip occurs is less than that for global slip by a factor $\chi_{PN}=1-k\lambda^2/(8g)$. This factor accounts for the nearest-neighbour interaction energy $\propto (1/2)k\lambda^2$. So $\chi_{PN}\to 1$ as $k\to 0$, recovering the global slip prediction.

The value for the Peierls–Nabarro transition is strictly valid only for the case in which the number of atoms is fixed. Furthermore, it relies on the forcing V in (4.1) being a fixed value. Neither of these conditions holds for a simulation or at a real boundary: vacancies are transitory, being created and annihilated as atoms depart or arrive from the bulk, and the forcing will fluctuate. We assume then, in using this value, that the vacancies are long-lived and (as noted in § 3.2) widely separated. And, we assume that using the mean value of V is representative of the fluctuating forcing.

The onset of defect slip, as for global slip, is expected over a range of wall speeds, due to the distribution of heights of the atoms in the first liquid layer. Here, we calculate the lowest value at which defect slip might be expected. (This suits the derivation for χ_{PN}, which is only valid for small V.) As those atoms held most weakly by the substrate will slip first, we evaluate $U_{PN}=\chi_{PN}(l)U_{GS}(l)$ at the height l at the outer edge of the first liquid layer, namely at (the location of the peak density, 0.34 nm) + (the half-width, 0.035 nm) yielding $U_{PN}\simeq 10\,\mathrm{m\,s^{-1}}$. This value is marked on figures 2, 4 and 5. It has the same order of magnitude as the observed onset of slip, but is higher than the observed onset in figure 5. As noted above, the vdFK model uses a one-dimensional solid surface in which the liquid atoms must pass over the maximum of the substrate potential in hopping from one equilibrium site to

another. In the MD simulation over a two-dimensional solid surface, liquid atoms can sidestep the maximum of the substrate potential. So, it can be expected that, as is the case here, the vdFK prediction overestimates the forcing required from the MD simulations.

4.3. *As the forcing becomes large, the slip length asymptotes to a constant value*

At very large forcing, the final two terms of (4.1) dominate, leading to the result $v_s = \eta_{LL} V/(\eta_{LL} + \eta_{LS})$ where, since all atoms have the same velocity, the individual $\dot{x}_i$ have been replaced by v_s. After using the definition of the slip length from § 2 and approximating the shear rate with $\dot{\gamma} = (V - v_s)/d$, we find

$$L_s = \frac{\eta_{LL}}{\eta_{LS}} d. \tag{4.3}$$

(It is a technical point that d, the distance between the first and second liquid layers, is differentiated from l, the distance to the first peak of the density; in fact, they are nearly equal in value (see also Koplik, Banavar & Willemsen 1989).) The slip length, then, should asymptote to a constant value in the limit of high forcing. We see from figure 5 that the slip lengths measured from the MD simulations agree with this prediction. In order to quantitatively compare the value predicted by (4.3) to the simulation results, (4.3) is evaluated using the length l and the bulk viscous coefficient η_{LL}; it is difficult to determine a precise value for η_{LS} (see Sokhan, Nicholson & Quirke 2001), though it is often found to be within an order of magnitude less than η_{LL} and is at most equal to η_{LL}. So, it is reasonable to expect $1 \leqslant L_s/l \leqslant 10$. (But, in some cases $\eta_{LS} \ll \eta_{LL}$, as in carbon nanotubes (see Majumder *et al.* 2005).) The best-fit zero-slope line to the data for $U > 20\,\mathrm{m\,s^{-1}}$ is $L_s/l = 5.2$ ($L_s = 1.75\,\mathrm{nm}$) which is within this predicted range.

5. Conclusions

That slip occurs in nano- and micro-scale liquid flows has been established by many experimental and computational studies. The work here presents evidence for the molecular mechanisms by which this slip occurs. In one form of slip, liquid atoms hop along the solid surface from one equilibrium site to another, passing through a higher-energy transition state. The equilibrium sites compose the ground state, which is shown to exist by measuring the variance. The hopping process follows Arrhenius dynamics, as expected for a rate process between equilibrium sites. Visual evidence indicates localized motion, as expected for a hopping process. Only a small percentage of the liquid atoms are hopping at any instant, validating the rate-process approach, which assumes that each rate process is affected only by the local dynamics. A second mechanism, global slip, relies on the participation of the entire liquid layer. The signature of this mode of slip is parallel trajectories of all the liquid atoms, as is observed at high enough forcing.

The vdFK model describes the dynamics of liquid atoms adjacent to a solid surface. It predicts a bifurcation at low forcing from no-slip to the solitonic propagation of defects over a corrugated potential. There is a second critical value of forcing past which there is global motion of the entire layer. The MD simulations qualitatively agree with the predictions of these transitions. The vdFK equation further predicts that the slip length should approach a constant value at extremely high levels of forcing, also in agreement with the MD data.

Though liquids are characterized by their disorder, the lattice of discrete solid atoms at a boundary induces order, tangentially along its surface, on the adjacent liquid.

This order needs to be strict enough to generate a ground state, yet fluid enough to permit the propagation of defects and the slipping of the entire layer. We imagine that the liquid–solid interface will continue to reveal a panoply of interesting behaviours arising from the balance of order and disorder.

The authors are grateful to the National Science Foundation for both financial support through the IGERT Program and computation support through TeraGrid resources provided by NCSA.

Appendix A. The random walk with a ground state

The number of atoms M in the first liquid layer is measured at each time step Δt for a total time t consisting of $N_t = t/\Delta t$ steps. The time step is chosen so that the change in M is $+1$, -1, or 0, with other values rarely occurring. R realizations are generated so the value ($+1$, -1, or 0) at each time step can be placed as the entry a_{ij} in an $N_t \times R$ matrix. Taking the cumulative total of a_{ij} after time $i\Delta t$ generates a new $N_t \times R$ matrix with entries $b_{ij} = \sum_{k=1}^{i} a_{kj}$. At each time step, the variance $\mathrm{Var}_i = \sum_{j=1}^{R} (b_{ij} - (1/R)\sum_{j=1}^{R} b_{ij})^2/R$ is computed.

If ($+1$, -1, 0) occur with fixed probabilities (p, q, τ), where $\tau = 1 - p - q$, then the variance increases linearly in time according to $\mathrm{Var}_i = 4ipq/(1-\tau)$. On the other hand, if there is a ground-state configuration then diffusion into and out of the first liquid layer will be affected. Consider that the first liquid layer is in its ground-state configuration, that is, at its lowest energy. Removing atoms from the ground-state configuration incrementally increases the energy. Hence, the cumulative total b_{ij} measures the distance from the energy minimum. In the limit of many steps, the discrete changes in b_{ij} can be modelled by a continuous distance x via the Smoluchowski equation,

$$\frac{\partial \mathscr{P}}{\partial t} = \frac{\partial}{\partial x}\left(\mathscr{P}\frac{\partial \phi}{\partial x}\right) + \frac{\partial^2 \mathscr{P}}{\partial x^2}, \tag{A 1}$$

for the probability $\mathscr{P}(x, t)$ of being distance x from the energy minimum of a potential ϕ. Note that, on the infinite line, for a constant potential, there is no steady-state solution, and $\mathscr{P}(x, t)$ continues to evolve and flatten out, leading to a linear increase in variance. On the other hand, if there is a ground state, which is most simply solved using a quadratic potential, then (A 1) has a steady-state solution. A time-invariant solution has time-invariant statistical measures, in particular a constant variance.

Appendix B. Amplitude of the wall potential

The amplitude of the wall potential, g, which appears in (4.1), is determined by first computing the potential at a point (x, l) a distance l above the solid array of Lennard–Jones atoms spaced λ in x and s in y,

$$V_{LJ}(x) = 4\epsilon_{LS} \sum_{i=0}^{M_L} \sum_{j=-M}^{M} \left[\left(\frac{\sigma}{r_{ji}}\right)^{12} - \left(\frac{\sigma}{r_{ji}}\right)^{6} \right], \tag{B 1}$$

where $r_{ji}^2 = (x - j\lambda)^2 + (l + is)^2$. The index j counts the $2M$ atoms along a particular layer, i indexes the M_L layers which are separated by distance s. The coefficients in (B 1) are the MD simulation parameters, as given in § 2. The cosine transform of $V_{LJ}(x)$ is computed and the coefficient for the lowest mode is set equal to g.

REFERENCES

Blake, T. D. 1990 Slip between a liquid and a solid: D. M. Tolstoi's (1952) theory reconsidered. *Colloids Surfaces* **47**, 135–145.

Bocquet, L. & Barrat, J.-L. 2007 Flow boundary conditions from nano- to micro-scales. *Soft Matter* **3**, 685693.

Braun, O. M. & Kivshar, Y. S. 1998 Nonlinear dynamics of the Frenkel–Kontorova model. *Phys. Rep.* **306**, 1–108.

Braun, O. M., Kivshar, Yu. S. & Zelenshkaya, I. I. 1990 Kinks in the Frenkel-Kontorova model with long-range interparticle interactions. *Phys. Rev.* B **41**, 7118–7138.

Eijkel, J. C. T. & van den Berg, A. 2005 Nanofluidics: What it is and what can we expect from it? *Microfluid. Nanofluid.* **1**, 249–267.

Floría, L. M. & Mazo, J. J. 1996 Dissipative dynamics of the Frenkel-Kontorova model. *Adv. Phys.* **45**, 505–598.

Glasstone, S., Laider, K. H. & Eyring, H. 1941 *The Theory of Rate Processes*. McGraw-Hill.

Hanggi, P., Talkner, P. & Borkovec, M. 1990 Reaction-rate theory: Fifty years after Kramers. *Rev. Mod. Phys.* **62**, 251–341.

Hoffman, R. L. 1983 A study of the advancing interface: II. Theoretical prediction of the dynamic contact angle in liquid-gas systems. *J. Colloid Interface. Sci.* **94**, 470–486.

Holt, J. K., Park, H. G., Wang, Y., Stadermann, M., Artyukhin, A. B., Grigoropoulos, C. P., Noy, A. & Bakajin, O. 2006 Fast mass transport through sub-2-nanometer carbon nanotubes. *Science* **312**, 1034–1037.

Horn, R. G. & Israelachvili, J. N. 1981 Direct measurement of structural forces between two surfaces in a nonpolar liquid. *J. Chem. Phys.* **75**, 1400–1411.

Koplik, J., Banavar, J. R. & Willemsen, J. F. 1989 Molecular dynamics of fluid flow at solid surfaces. *Phys. Fluids* A **1**, 781–794.

Lauga, E., Brenner, M. P. & Stone, H. A. 2005 Microfluidics: The no-slip boundary condition. In *Handbook of Experimental Fluid Dynamics* (ed. J. Foss, C. Tropea & A. Yarin), chap. 15. Springer.

Lichter, S., Martini, A., Snurr, R. Q. & Wang, Q. 2007 Liquid slip as a rate process. *Phys. Rev. Lett.* **98**, 226001.

Lichter, S., Roxin, A. & Mandre, S. 2004 Mechanisms for liquid slip at solid surfaces. *Phys. Rev. Lett.* **93**, 086001.

Majumder, M., Chopra, N., Andrews, R. & Hinds, B. J. 2005 Nanoscale hydrodynamics: enhanced flow in carbon nanotubes. *Nature* **438**, 44.

Martini, A., Liu, Y. C., Snurr, R. Q. & Wang, Q. 2006 Molecular dynamics characterization of thin film viscosity for EHL simulation. *Tribol. Lett.* **21**, 217–225.

Neto, C., Evans, D. R., Bonaccurso, E., Butt, H.-J. & Craig, V. S. J. 2005 Boundary slip in Newtonian liquids: A review of experimental studies. *Rep. Prog. Phys.* **68**, 2859–2897.

Roxin, A. 2004 Five projects in pattern formation, fluid dynamics, and computational neuroscience. PhD thesis, Northwestern University.

Sholl, D. S. & Johnson, J. K. 2006 Making high-flux membranes with carbon nanotubes. *Science* **312**, 1003–1004.

Sokhan, V. P., Nicholson, D. & Quirke, N. 2001 Fluid flow in nanopores: An examination of hydrodynamic boundary conditions. *J. Chem. Phys.* **115**, 3878–3887.

Steele, W. A. 1973 The physical interaction of gases with crystalline solids. *Surface Sci.* **36**, 317–352.

Thompson, P. A. & Robbins, M. O. 1990 Shear flow near solids: Epitaxial order and flow boundary conditions. *Phys. Rev.* A **41**, 6830–6837.

Thompson, P. A. & Troian, S. M. 1997 A general boundary condition for liquid flow at solid surfaces. *Nature* **389**, 360–362.

Urbakh, M., Klafter, J., Gourdon, D. & Israelachvili, J. 2004 The nonlinear nature of friction. *Nature* **430**, 525–528.

Zhu, Y. & Granick, S. 2002 Limits of the hydrodynamics no-slip boundary condition. *Phys. Rev. Lett.* **88**, 106102.